

Quantum statistics of Schrödinger cat states prepared by logical gate with non-Gaussian resource state

N. I. Masalaeva and I. V. Sokolov*

Saint Petersburg State University, Universitetskaya nab. 7/9, 199034 Saint Petersburg, Russia

A measurement-induced continuous-variable logical gate is able to prepare Schrödinger cat states if the gate uses a non-Gaussian resource state, such as cubic phase state [I. V. Sokolov, Phys. Lett. A **384**, 126762 (2020)]. Our scheme provides an alternative to hybrid circuits which use photon subtraction and (or) Fock resource states and photon number detectors. We reveal the conditions under which the gate conditionally prepares quantum superposition of two undistorted “copies” of an arbitrary input state that occupies a finite area in phase space. A detailed analysis of the fidelity between the gate output state and high-quality Schrödinger cat state is performed. A clear interpretation of the output state quantum statistics in terms of Wigner function in dependence on the gate parameters and measurement outcome is presented for a representative set of input Fock states.

I. INTRODUCTION

The continuous-variable (CV) quantum information schemes based on Gaussian resource states were extensively explored both theoretically and experimentally [1–4], including their essentially multimode implementation [5–9]. While the continuous-variable Gaussian cluster schemes are able to perform Gaussian transformations of the input states, in order to achieve universal quantum computing, there is a need to introduce the non-Gaussian logical gates [1, 2].

A minimal nonlinearity sufficient to prepare non-Gaussian resource states is cubic. The cubic phase state based on the cubic nonlinearity was first considered in [10, 11]. Various approaches to the implementation of such states, as well as of the cubic (or higher) phase gates, were explored both theoretically and experimentally [12–17].

It was shown recently [18], that continuous-variable measurement-induced two-node logical gate is able to prepare Schrödinger cat-like quantum superpositions, if Gaussian (e. g. squeezed) resource state of an ancillary oscillator is substituted with non-Gaussian one. This was demonstrated for the cubic phase state used as a resource.

An important distinction between the gate [18] and the non-Gaussian circuits mentioned above is that the Schrödinger cat state emerges when the ancillary oscillator measurement is compatible not with one, but with two different values of the target oscillator physical variables. This feature does not appear in Gaussian quantum networks and, given that a non-Gaussian resource state is used, needs the measurement which is consistent with this criterion.

In general, one can prepare CV Schrödinger cat states by making use of the unitary evolution assisted by a nonlinear interaction [19]. The schemes based on a hybrid measurement-induced evolution also can create cat-like

states. The optical Schrödinger cat states were generated in a low-photon regime using photon subtraction [20], the homodyne detection with photon number state as a resource [21], and the iterative schemes which allow an incremental enlargement of cat states [22–24]. The latter proposals are specifically aimed at the creation of superpositions of two coherent states. The Schrödinger cat states can be prepared by using a photonic even-parity detector and CV entanglement [25].

The Schrödinger cat states are an object of relentless interest since their first introduction [26]. Besides their fundamental importance, some proposals for fault-tolerant quantum information processing directly rely on the cat-like states [10, 27].

In this work, we explore in detail the quantum statistics of the superpositions, which are prepared by our gate from an arbitrary input state that occupies a limited area in phase space. Of interest is the gate operation regime, where the gate output state is close to “perfect” Schrödinger cat state, that is, to the superposition of two symmetrically displaced undistorted copies of the input state. By considering the fidelity between the actual gate output state and the needed form of cat state, we find the conditions under which the gate prepares high-quality cat states.

We present the output states Wigner functions for a wide range of the gate parameters and reveal the connection between the fidelity and the shape of the input state copies support in phase space.

While the gate is universal and can prepare Schrödinger cat states from almost arbitrary input states, the quality of the output states depends on the input states extent along the coordinate and momentum axes. We consider input Fock states with up to two photons and demonstrate the gate potential to prepare high-quality cat-like superpositions out of these and similar states.

Note that considerable efforts have been made to generate superpositions of coherent states with large enough distance between the components [20–24]. The gate based on the cubic phase state can prepare such super-

*Electronic address: i.sokolov@spbu.ru, sokolov.i.v@gmail.com

positions with as large as needed distance between the copies in phase space.

Our analysis is based on the exact form of the output state [18]. At the same time, the gate operation may be illustrated in terms of an approximate visual representation of the step-by-step quadrature amplitudes transformations in the scheme if one considers these transformations in a semiclassical manner. This approach gives a clear idea how Schrödinger cat states may emerge in similar circuits. It might be useful for the analysis of logical gates based on more complex non-Gaussian resource states, where exact solution is not available.

II. CAT-LIKE STATES FROM CV GATE WITH NON-GAUSSIAN RESOURCE STATE

The non-Gaussian gate we discuss here was introduced in [18]. The measurement-induced two-node gate uses the cubic phase state as an elementary non-Gaussian resource, the entangling C_Z operation, and the projecting homodyne measurement.

A key feature of the gate is that the measurement outcome provides multivalued information about the output state canonical variables, which results in the preparation of a cat-like state. This feature is interpreted in the next section in terms of a clear pictorial representation.

Let us outline briefly the gate operation (for more details see [18]). The target oscillator is initially prepared in an arbitrary state

$$|\psi_1\rangle = \int dx_1 \psi(x_1) |x_1\rangle,$$

which is assumed to occupy a limited range $\{\Delta x_1, \Delta y_1\}$ of the coordinate and momentum. In order to prepare the non-Gaussian resource state of the ancillary oscillator, one applies unitary non-Gaussian evolution operator $\exp(i\gamma q_2^3)$ to the momentum eigenstate $|0\rangle_{p_2}$,

$$|\psi_2\rangle = e^{i\gamma q_2^3} |0\rangle_{p_2} = \int dx_2 e^{i\gamma x_2^3} |x_2\rangle.$$

In the following, we use the notation $\{q, p\}$ for the coordinate and momentum operators.

The C_Z entangling unitary evolution operator $\exp(iq_1 q_2)$ prepares the state

$$|\psi_{12}\rangle = \int dx_1 dx_2 \psi(x_1) e^{ix_2(x_1 + \gamma x_2^2)} |x_1\rangle |x_2\rangle. \quad (1)$$

Next, the ancillary oscillator momentum is measured with the outcome y_m . Projecting the state (1) on the homodyne detector eigenstate $|y_m\rangle_{p_2}$, one arrives at target oscillator output state

$$\psi^{(out)}(x) = \sqrt{\mathcal{N}} \psi(x) \varphi(x - y_m), \quad (2)$$

where $x_1 \rightarrow x$ for brevity, and \mathcal{N} is the normalization factor. As the result of gate operation, the input state is

multiplied by the factor

$$\begin{aligned} \varphi(x - y_m) &= \frac{1}{\sqrt{2\pi}} \int dx' e^{ix'(x - y_m + \gamma x'^2)} \\ &= [\sqrt{2\pi}/(3\gamma)^{1/3}] \text{Ai}[(x - y_m)/(3\gamma)^{1/3}], \end{aligned} \quad (3)$$

which is expressed in terms of the Airy function.

While the result (2), (3) is exact, it is instructive to consider the approximation where one can specify two stationary phase points of the exponent in (3). In this approximation, the added factor becomes a sum of two contributions which directly correspond to the components of the output quantum superposition. In the following, we demonstrate that cat-like states arise just if this approximation is valid.

For a given target oscillator coordinate x , the stationary points are

$$x'_{st} = \pm \sqrt{(y_m - x)/3\gamma}. \quad (4)$$

If two stationary phase points exist for all x within the region spanned by the input state, we finally arrive at the approximate output state

$$\psi_{st}^{(out)}(x) = \sqrt{\mathcal{N}_{st}} \psi(x) [\varphi^{(+)}(x - y_m) + c.c.], \quad (5)$$

where \mathcal{N}_{st} is the normalization factor, and

$$\begin{aligned} \varphi^{(+)}(x - y_m) &= \exp \left\{ i \left[\frac{\pi}{4} - \frac{2}{3\sqrt{3\gamma}} (y_m - x)^{3/2} \right] \right\} \\ &\quad \times [12\gamma(y_m - x)]^{-1/4}. \end{aligned} \quad (6)$$

In Fig. 1 we plot the infidelity $1 - F_{st}$ between the exact solution (2) and the output state (5) evaluated in the stationary phase approach, where the fidelity is

$$F_{st} = \left| \int dx \psi^{(out)*}(x) \psi_{st}^{(out)}(x) \right|^2. \quad (7)$$

As the input states of the target oscillator, we choose here the first Fock states $|n\rangle$ with the coordinate wave function

$$\psi_n^F(x) = \frac{1}{\pi^{1/4} \sqrt{2^n n!}} H_n(x) e^{-x^2/2}, \quad (8)$$

where $H_n(x)$ is the Hermite polynomial, and $n = 0, 1, 2$ correspondingly.

If the input state probability distribution is concentrated within a certain range $-\Delta x \leq x \leq \Delta x$, and the measured ancilla momentum is not large enough, $y_m \leq \Delta x$, there are coordinates x such that two distinct stationary phase points do not exist, see (4). For the vacuum input state one can assume $\Delta x \rightarrow 1$. The fidelity (7) for $y_m \leq 1$ is low, as seen from the Fig. 1(a). At the same time, beyond the region $y_m \leq 1$ the stationary phase approach provides higher fidelities.

For the input Fock states $|n\rangle$ with $n = 1$ and 2 , better fidelities are achieved in the area $y_m \geq \sqrt{2n+1}$, see Fig. 1(b, c), in agreement with the estimate $\Delta x \sim \sqrt{2n+1}$.

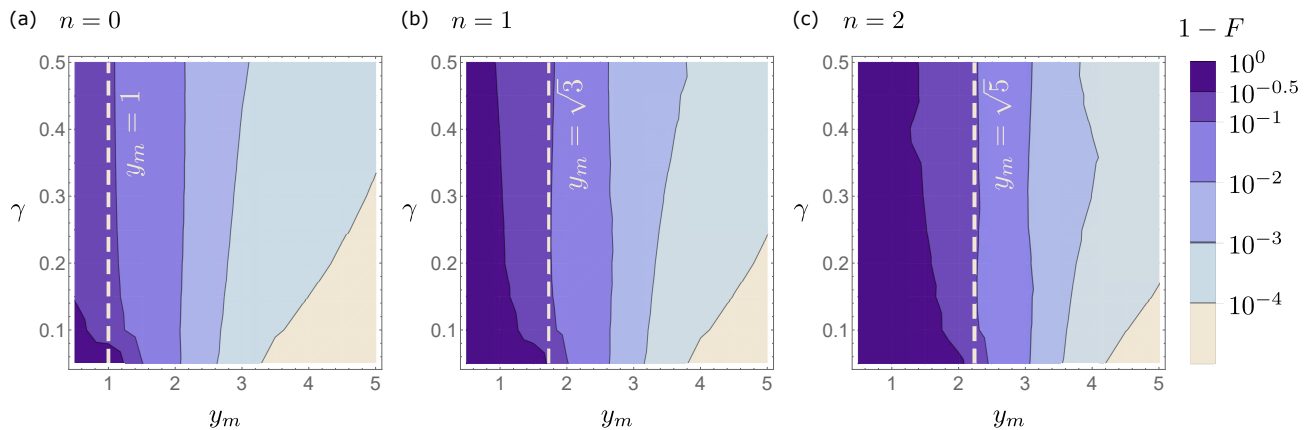


FIG. 1: Infidelity between the exact solution (2) for the output state and the output state (5) evaluated in the stationary phase approach. The input states are Fock states with $n = 0, 1, 2$ quanta correspondingly. The vertical dashed lines $y_m = \sqrt{2n+1}$ separate the areas where the stationary phase approach does not work.

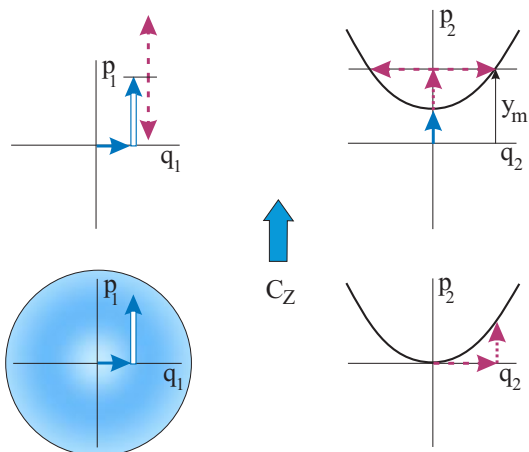


FIG. 2: Measurement-induced evolution of quadrature amplitudes of the target (left) and ancillary (right) oscillators. The randomly chosen initial amplitudes undergo the transformation of the cubic phase state preparation (bottom right), the entangling non-demolition C_Z operation, and the ancilla momentum measurement with the outcome y_m (top right). The target oscillator state collapses to the cat-like state (top left).

III. INPUT STATE EVOLUTION IN PHASE SPACE

There is a clear pictorial representation [18] in phase space of the evolution performed by the gate, illustrated in Fig. 2. The scheme shows the step-by-step transformation of the target and ancillary oscillators quadrature amplitudes $\{q_i, p_i\}$, where $i = 1, 2$, as these transformations arise in the Heisenberg picture under some simplifying admissions.

The initial canonical variables of both nodes of our scheme are denoted via $\{q_i(0), p_i(0)\}$. The ancilla cubic phase state is prepared by the non-Gaussian unitary

evolution operator $\exp(i\gamma q_2^3)$ applied to the initial ancilla momentum eigenstate $|0\rangle_{p_2}$. The Heisenberg equations for canonical variables solved on unit time interval with the Hamiltonian $-\gamma q_2^3$ yield,

$$\begin{aligned} q_1 &= q_1(0), & q_2 &= q_2(0), \\ p_1 &= p_1(0), & p_2 &= p_2(0) + 3\gamma q_2^2(0). \end{aligned} \quad (9)$$

Next, the two-node entangling evolution $\exp(iq_1q_2)$ (the non-demolition C_Z operation) is applied, which adds coordinate of the 1st oscillator to the momentum of the 2nd, and vice versa. The canonical variables in the entangled state are found to be

$$\begin{aligned} q_1^e &= q_1(0), \\ p_1^e &= p_1(0) + q_2(0), \end{aligned} \quad (10)$$

$$\begin{aligned} q_2^e &= q_2(0), \\ p_2^e &= p_2(0) + 3\gamma q_2^2(0) + q_1(0). \end{aligned}$$

In Fig. 2, we represent these transformations by randomly choosing initial points in phase space for both oscillators within the region spanned by the corresponding statistical ensemble. The initial ancilla state $|0\rangle_{p_2}$ with zero momentum uncertainty may be represented by a horizontal line. The transformation (9) prepares the well-known non-Gaussian cubic phase state [10, 11] (up to the $q \leftrightarrow p$ substitute), whose Wigner function demonstrates fringes and negativity [12], and the Wigner logarithmic negativity is almost maximal among some elementary non-Gaussian states [28].

Nevertheless, the gate under consideration can be effectively described if the transformations (9), (10) and (11) (see below) are treated in a semiclassical manner, that is, when it is admitted that one can put in correspondence a certain value of momentum to any given coordinate. In this approximation, the horizontal line which represents the ancilla initial state is mapped point-by-point by the transformation (9) to the parabola shown in Fig. 2 (bottom right).

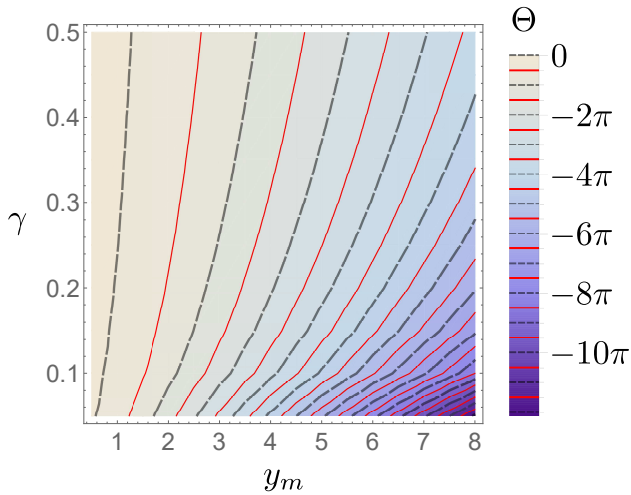


FIG. 3: Phase θ (13) as a function of the gate parameters γ and measurement outcome y_m . The black dashed and red solid lines correspond to even and odd cat states, respectively.

The ancilla momentum measurement with the outcome y_m imposes links to the possible values of the coordinates and momenta, as shown in Fig. 2 (top right). By substituting the observed momentum value y_m for p_2^e , one arrives at the following measurement-induced target oscillator quadrature amplitudes, depicted in the same figure (top left),

$$\begin{aligned} q_1^{(out)} &= q_1(0), \\ p_1^{(out)} &= p_1(0) \pm (3\gamma)^{-1/2} \sqrt{y_m - q_1(0) - p_2(0)}. \end{aligned} \quad (11)$$

In view of $p_2(0)|0\rangle_{p_2} = 0$, one can drop $p_2(0)$ here.

In general, substituting the measurement outcome for the relevant operator-valued observable in the Heisenberg picture may ruin the commutation relations. As far as the output variables are multivalued in our scheme, the result (11) can not be considered as exact in the Heisenberg picture.

Nevertheless, the output amplitudes (11) agree not only with the semiclassical visualization in phase space of the transformation performed by the gate but also with the solution (5), as we demonstrate below. Note that two distinct values of the output oscillator momentum arise just if there are two distinct stationary phase points. The distance between two values of x'_{st} (which are eventually mapped to the output momentum due to the entanglement), and between two values of $p_1^{(out)}$ in (11) is given by the same expression for any output coordinate.

That is, there is a direct correspondence between the Heisenberg-like picture we discuss here and its visualization on the one hand, and the solution derived in the stationary phase approximation on the other hand.

In general, a cat-like state is prepared when the ancilla measurement outcome is compatible with two or more distinct values of the target oscillator variables. This feature does not arise in the Gaussian measurement-induced

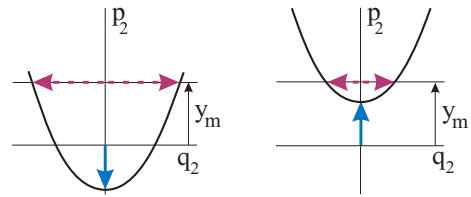


FIG. 4: The measurement-induced splitting of the observed ancilla coordinate (dashed arrows) for different values of the target oscillator coordinate q_1 (solid arrows).

CV schemes since it is due to the non-linear deformation of the resource state in phase space. With the cubic phase state used as a non-Gaussian resource, two “copies” of an input state may be created by the gate, as seen from (6) and (11).

IV. QUANTUM STATISTICAL PROPERTIES OF THE OUTPUT SCHRÖDINGER CAT STATES

In this section, we discuss the potential of our scheme to prepare “perfect” cat states, where two components of the output superposition are undistorted copies of the input state symmetrically displaced in phase space along the momentum axis.

For the input state whose coordinate wave function is concentrated around $x = 0$, one can Taylor expand the added factor (6) in x . In the linear in x approximation for the exponent, we arrive at

$$\varphi^{(+)} \rightarrow \varphi_{cat}^{(+)} = \exp[i(\theta + p^{(+)}x)](12y_m\gamma)^{-1/4}, \quad (12)$$

where

$$\theta = \frac{\pi}{4} - \frac{2}{3\sqrt{3\gamma}}y_m^{3/2}, \quad p^{(+)} = \sqrt{y_m/3\gamma}. \quad (13)$$

Here $p^{(+)}$ is the displacement of a copy due to the factor $\varphi^{(+)}$.

Consider cat state preparation from the input Fock state (8). In the approximation adopted here, the output state coordinate wave function is given by

$$\psi_{n,cat}^{(out)}(x) = \sqrt{\mathcal{N}_{n,cat}} \cos(\theta + \sqrt{y_m/3\gamma}x) H_n(x) e^{-x^2/2}, \quad (14)$$

where $\mathcal{N}_{n,cat}$ is the normalization factor. In particular, the displaced vacuum input state may be represented in terms of the Glauber state $|\alpha\rangle$ as

$$\exp[i(\theta + \sqrt{y_m/3\gamma}x)]\psi_0^F(x) \leftrightarrow e^{i\theta}|\alpha\rangle,$$

where $\alpha = i\sqrt{y_m/6\gamma}$. Hence, the Schrödinger cat state produced from the vacuum one is

$$\sqrt{\mathcal{N}_{vac}}(e^{i\theta}|\alpha\rangle + e^{-i\theta}|-\alpha\rangle), \quad (15)$$

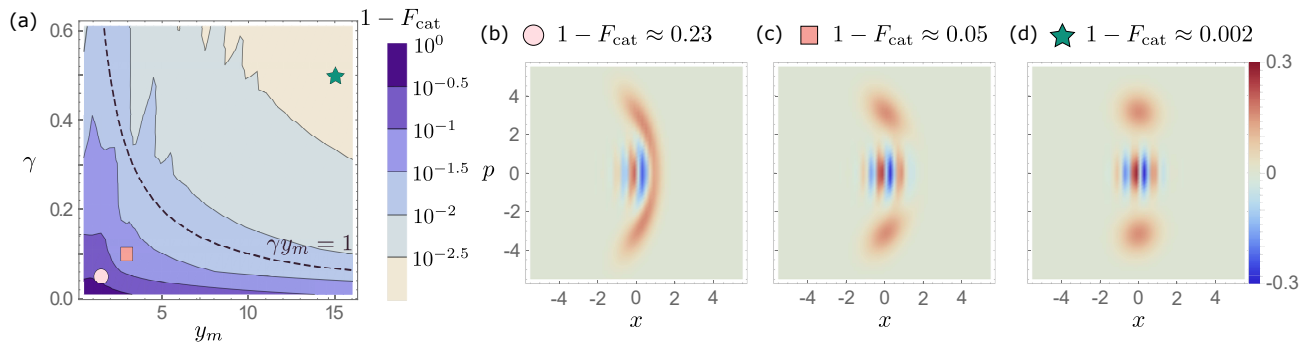


FIG. 5: Infidelity $1 - F_{cat}$ (a) between the exact output state (2) and “perfect” cat state (14) for vacuum input state of the target oscillator as a function of the gate parameter γ and measurement outcome y_m . The Wigner function of the exact output state for the points $\{y_m, \gamma\}$ indicated by the circle (b), square (c), and asterisk (d), respectively.

where

$$\mathcal{N}_{vac}^{-1} = 2[1 + \cos(2\theta)e^{-2|\alpha|^2}].$$

In the coordinate representation, the state (15) is

$$\psi_{0,cat}^{(out)}(x) = \frac{\sqrt{2}}{\pi^{1/4}} \frac{\cos(\theta + \sqrt{y_m/3}\gamma x)}{\sqrt{(1 + \cos(2\theta)e^{-y_m/3\gamma})}} e^{-x^2/2}. \quad (16)$$

Given that the approximation (12) is valid, an arbitrary input state is transformed by the gate to the cat-like superposition of two undistorted copies symmetrically shifted along the momentum axis, in analogy to (14) and (15). The phase θ (13) which determines the relative phase shift of the cat state components is depicted in Fig. 3 as a function of the gate parameters and measurement outcome. The emerging cat state is even for $\theta = m\pi$ and odd for $\theta = (m + 1/2)\pi$ with m integer.

It is instructive to evaluate the deformation of the cat state components and to reveal optimal conditions under which the gate prepares “perfect” Schrödinger cat states. In Fig. 4, we illustrate how such deformation arises for the cubic phase state used as a non-Gaussian resource state in our scheme. This figure reproduces the top right part of Fig. 2 for different target oscillator coordinates. As seen from Fig. 4, for a given ancilla momentum measurement outcome, the arising splitting of the observed ancilla coordinate may essentially depend on the target oscillator coordinate.

In order to estimate the linear shearing deformation of the copies, we take into account the next term in the Taylor expanded phase of the added factor (6),

$$\varphi^{(+)} \sim \exp\left\{i[\theta + (p^{(+)} + \delta p^{(+)}(x))x]\right\},$$

where

$$\delta p^{(+)}(x) \approx -\frac{1}{4\sqrt{3}\gamma y_m}x.$$

Consider an input state which spans a range $2\Delta x$ along the coordinate axis. The linear in x contribution

$|\delta p^{(+)}(x)|$ to the momentum of a copy changes at the distance $2\Delta x$ as

$$|\Delta(\delta p^{(+)}(x))| \sim \lambda \cdot 2\Delta x,$$

where the parameter

$$\lambda = \frac{1}{4\sqrt{3}\gamma y_m} \sim \frac{0.14}{\sqrt{\gamma y_m}}, \quad (17)$$

can be viewed as a measure of the linear shearing deformation.

In Figs. 5(a) and 6(a,e) we represent the infidelity $1 - F_{cat}$ between the exact output state (2) and “perfect” cat state (14), where

$$F_{cat} = \left| \int dx \psi^{(out)*}(x) \psi_{cat}^{(out)}(x) \right|^2, \quad (18)$$

for input Fock states (8) with $n=0$ and $n=1, 2$, respectively. In these figures, we also plot the curves $\gamma y_m = 1$, thus separating the areas of “large” ($\lambda \geq 0.14$) and “small” ($\lambda \leq 0.14$) deformation of the cat state components.

As seen from the figures, the fidelity F_{cat} dependence on the gate parameters and measurement outcome is in a good agreement with the estimate given above, and the gate output may be very close to the “perfect” cat state.

In order to show how the output state looks like for the cases of bad, fair, and good fidelity (18), we plot in Figs. 5(b,c,d), 6(b,c,d), and 6(f,g,h) the corresponding output state Wigner functions evaluated using the exact solution (3). The points in the plane $\{y_m, \gamma\}$ indicated by a circle, square, and asterisk, respectively, are chosen in the regions of a bad, fair, and good fidelity.

Consider first the vacuum input state, Fig. 5(b,c,d). The points in the plane $\{y_m, \gamma\}$ for which the Wigner function was evaluated, are $\{1.5, 0.05\}$, $\{3, 0.1\}$, and $\{15, 0.5\}$. For these points, the average shift $p^{(+)} = \sqrt{y_m/3}\gamma$ of a copy along the momentum axis is equal to 3.16. This shift is larger than the input state spread in phase space, and one may consider the output state

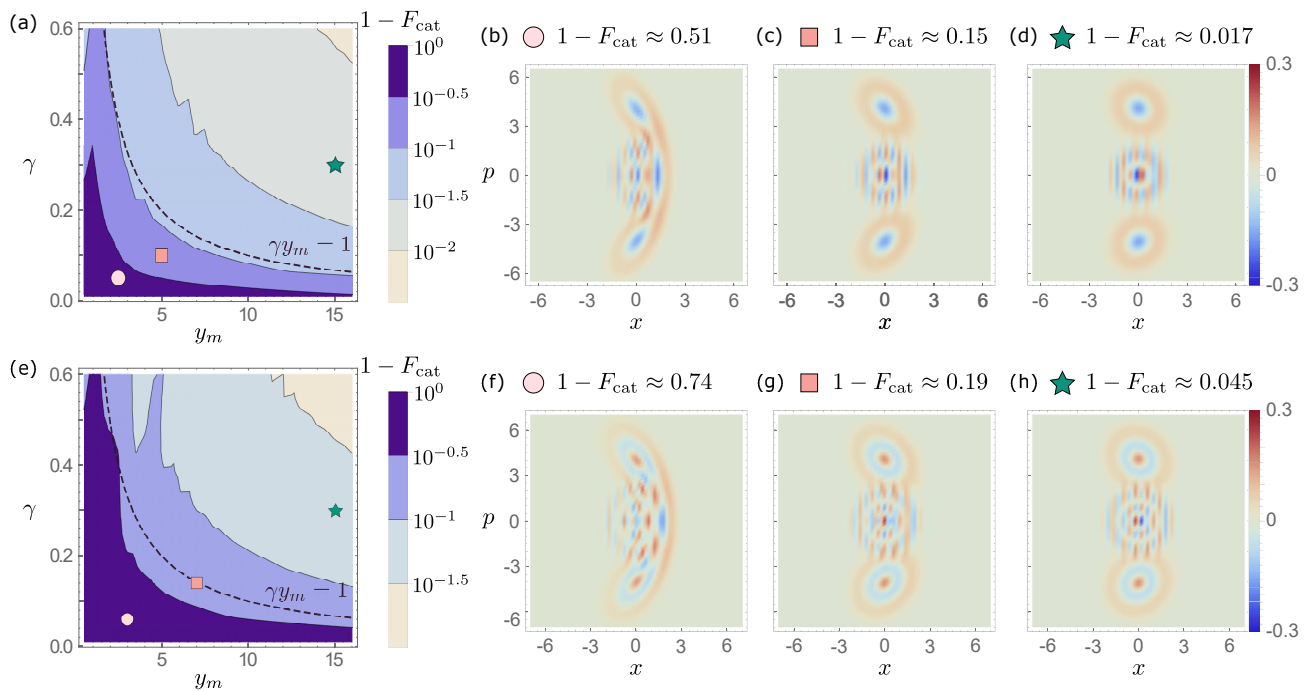


FIG. 6: Infidelity $1 - F_{cat}$ between the exact output state (3) and “perfect” cat state (14) for the single-photon (a) and two-photon (e) input state as a function of the gate parameter γ and measurement outcome y_m . The Wigner function of the exact output state for the single-photon (b,c,d) and two-photon (f,g,h) input states for the points $\{y_m, \gamma\}$ indicated by the circle, square, and asterisk, respectively.

as a “real” cat as opposed to “kittens” with small copies separation [20].

The Wigner function depicted in Fig. 5(b) was evaluated for $\{y_m, \gamma\} = \{1.5, 0.05\}$ and $F_{cat} = 0.77$. For this point, the fidelity F_{st} between the exact solution and the solution based on the stationary phase approach is low (see Fig. 1(a)), and even within the latter approach, the deformation parameter (17) is large enough, $\lambda \approx 0.51$. Fig. 5(b) shows that the support of the output state Wigner function is split by the gate, but its shape hardly corresponds to “perfect” cat state.

The Wigner function shown in Fig. 5(c) was evaluated for $\{y_m, \gamma\} = \{3, 0.1\}$ and $F_{cat} = 0.946$. The plot demonstrates well separated but distorted copies of the input state. Finally, in Fig. 5(d) we depict the output state Wigner function for $\{y_m, \gamma\} = \{15, 0.5\}$, where high fidelity $F_{cat} = 0.998$ is achieved, and the gate prepares the cat-like superposition close to the “perfect” cat state (15).

If the input Fock state is single- or two-photon, the gate is also able to prepare good cat states as shown in Figs. 6(b,c,d) and 6(f,g,h). Since $\Delta x \sim \sqrt{2n+1}$, we choose for these states such parameters of the gate that ensure sufficient separation of the copies.

For the single-photon input state (Figs. 6(b,c,d)), we take for $\{y_m, \gamma\}$ the values $\{2.5, 0.05\}$, $\{5, 0.1\}$, and $\{15, 0.3\}$. The copy shift along the momentum axis is $p^{(+)} = 4.08$. This gives $F_{cat} = 0.49, 0.85,$ and $0.983,$

respectively.

The Wigner functions for the two-photon input state (Figs. 6(f,g,h)) are plotted for the copy shift of $p^{(+)} = 4.08$. The parameters $\{y_m, \gamma\}$ are $\{3, 0.06\}$, $\{7, 0.14\}$, and $\{15, 0.3\}$, with $F_{cat} = 0.26, 0.81,$ and $0.955,$ respectively.

In general, our results show that the non-Gaussian gate under consideration is able to effectively prepare Schrödinger cat states from arbitrary input state, which occupies a finite range in phase space. As a “perfect” cat state, we imply here quantum superposition of undistorted copies of the input state displaced by $\pm p^{(+)}$ along the momentum axis, where the superposition components acquire phase factors $\exp(\pm i\theta)$, see (13).

The criterion of how close is the gate output state to the “perfect” cat state is given by the fidelity F_{cat} (18). As it follows from Figs. 5(d), 6(d), and 6(h), the fidelity F_{cat} decreases with the spread $2\Delta x$ of the input state coordinate. This may be attributed to the increasing role of deformations due to higher degrees of x , omitted in the Taylor expanded output state wave function (5) and (6). On the other hand, in order to improve the prepared cat state quality, one can choose the adequate gate parameters from the fidelity F_{cat} plots shown above.

Conclusion

We presented a detailed analysis of quantum statistical properties of the Schrödinger cat states prepared by the continuous-variable non-Gaussian gate. We have shown that the measurement-induced gate based on the cubic phase state is able to produce conditionally the superpositions of two “copies” of an arbitrary input state that occupies a finite area in phase space. The distance between the copies can be done as large as needed by a proper choice of the gate parameters. The cat states quality is characterized by the fidelity between the gate output state and the superposition of two symmetrically displaced undistorted copies of the input state. We found criteria for the gate operation with high fidelity, and illustrated qualitative behavior of the output cat states in terms of their Wigner functions for a wide range of parameters.

The gate exploits the same key elements, that is, the ancillary cubic phase state, the entangling C_Z operation, and homodyne measurement, as some other non-Gaussian CV schemes. A key feature of the regime where the cat-like states arise is that the measurement provides multivalued information about the target system physical variables. One can infer from our analysis that this fea-

ture may arise with other non-Gaussian resource states, and with other types of measurements. This makes our approach potentially scalable and extendable to more complex non-Gaussian networks.

The cat-breeding transformations of an arbitrary input state may be combined with standard Gaussian operations such as displacement, rotation, squeezing, and shearing deformation. By establishing the measurement window with a needed precision (which has effect on the success probability), one can conditionally generate complex cat-like structures in phase space. The multi-component Schrödinger cat states are considered [10, 27] as the logical qubit basis that ensures protection against errors of different origin.

In general, we expect that a CV quantum network with embedded non-Gaussian gates of a general kind may experience measurement-induced evolution to a Schrödinger cat state of an arbitrary complexity.

Acknowledgments

This research was supported by the Russian Foundation for Basic Research (RFBR) under the project 19-02-00204-a.

-
- [1] S. Lloyd and S. L. Braunstein. Quantum computation with continuous variables, *Phys. Rev. Lett.* **82**, 1784 (1999).
 - [2] S. L. Braunstein and P. van Loock. Quantum information with continuous variables, *Rev. Mod. Phys.* **77**, 513 (2005).
 - [3] A. Furusawa, J. L. Sørensen, S. L. Braunstein, C. A. Fuchs, H. J. Kimble, and E. S. Polzik. Unconditional quantum teleportation, *Science* **282**, 706 (1998).
 - [4] X. Li, Q. Pan, J. Jing, J. Zhang, C. Xie, and K. Peng. Quantum dense coding exploiting a bright Einstein-Podolsky-Rosen beam, *Phys. Rev. Lett.* **88**, 047904 (2002).
 - [5] M. Gu, C. Weedbrook, N. C. Menicucci, T. C. Ralph, and P. van Loock. Quantum computing with continuous-variable clusters, *Phys. Rev. A* **79**, 062318 (2009).
 - [6] C. Weedbrook, S. Pirandola, R. Garcia-Patron, N. J. Cerf, T. C. Ralph, J. H. Shapiro, and S. Lloyd. Gaussian quantum information, *Rev. Mod. Phys.* **84**, 621 (2012).
 - [7] R. Ukai, *Multi-Step Multi-Input One-Way Quantum Information Processing with Spatial and Temporal Modes of Light* (Springer, Tokyo, 2015).
 - [8] S. Yokoyama, R. Ukai, S. C. Armstrong, C. Sornphiphathphong, T. Kaji, S. Suzuki, J. Yoshikawa, H. Yonezawa, N. C. Menicucci, and A. Furusawa. Ultra-large-scale continuous-variable cluster states multiplexed in the time domain, *Nat. Photonics* **7**, 982 (2013).
 - [9] J. Roslund, R. Medeiros de Araújo, S. Jiang, C. Fabre, and N. Treps. Wavelength-multiplexed quantum networks with ultrafast frequency combs, *Nat. Photonics* **8**, 109 (2014).
 - [10] D. Gottesman, A. Kitaev, and J. Preskill. Encoding a qubit in oscillator, *Phys. Rev. A* **64**, 012310 (2001).
 - [11] S. D. Bartlett and B. C. Sanders. Universal continuous-variable quantum computation: Requirement of optical nonlinearity for photon counting, *Phys. Rev. A* **65**, 042304 (2002).
 - [12] S. Ghose and B. C. Sanders. Non-Gaussian ancilla states for continuous variable quantum computation via Gaussian maps, *J. Mod. Opt.* **54**, 855 (2007).
 - [13] P. Marek, R. Filip, and A. Furusawa. Deterministic implementation of weak quantum cubic nonlinearity, *Phys. Rev. A* **84**, 053802 (2011).
 - [14] M. Yukawa, K. Miyata, H. Yonezawa, P. Marek, R. Filip, and A. Furusawa. Emulating quantum cubic nonlinearity, *Phys. Rev. A* **88**, 053816 (2013).
 - [15] K. Marshall, R. Pooser, G. Siopsis, and C. Weedbrook. Repeat-until-success cubic phase gate for universal continuous-variable quantum computation, *Phys. Rev. A* **91**, 032321 (2015).
 - [16] K. Miyata, H. Ogawa, P. Marek, R. Filip, H. Yonezawa, J.-I. Yoshikawa, and A. Furusawa. Implementation of a quantum cubic gate by adaptive non-Gaussian measurement, *Phys. Rev. A* **93**, 022301 (2016).
 - [17] P. Marek, R. Filip, H. Ogawa, A. Sakaguchi, S. Takeda, J.-I. Yoshikawa, and A. Furusawa. General implementation of arbitrary nonlinear quadrature phase gates, *Phys. Rev. A* **97**, 022329 (2018).
 - [18] I. V. Sokolov. Schrödinger cat states in continuous variable non-Gaussian networks, *Phys. Lett. A* **384**, 126762 (2020).
 - [19] B. Yurke and D. Stoler. Generating quantum mechanical superpositions of macroscopically distinguishable states

- via amplitude dispersion, *Phys. Rev. Lett.* **57**, 13 (1986).
- [20] A. Ourjoumtsev, R. Tualle-Brouri, J. Laurat, and P. Grangier. Generating optical Schrödinger kittens for quantum information processing, *Science* **312**, 83 (2006).
- [21] A. Ourjoumtsev, H. Jeong, R. Tualle-Brouri, and P. Grangier. Generation of optical “Schrödinger cats” from photon number states, *Nature* **448**, 784 (2007).
- [22] J. Etesse, R. Blandino, B. Kanseri, and R. Tualle-Brouri. Proposal for a loophole-free violation of Bell’s inequalities with a set of single photons and homodyne measurements, *New J. Phys.* **16**, 053001 (2014).
- [23] J. Etesse, M. Bouillard, B. Kanseri, and R. Tualle-Brouri. Experimental generation of squeezed cat states with an operation allowing iterative growth, *Phys. Rev. Lett.* **114**, 193602 (2015).
- [24] D. V. Sychev, A. E. Ulanov, A. A. Pushkina, M. W. Richards, I. A. Fedorov, and A. I. Lvovsky. Enlargement of optical Schrödinger cat states, *Nat. Photonics* **11**, 379 (2017).
- [25] G. S. Thekaddath, B. A. Bell, I. A. Walmsley, and A. I. Lvovsky. Engineering Schrodinger cat states with a photonic even-parity detector, *Quantum* **4**, 239 (2020).
- [26] E. Schrödinger. Die gegenwärtige Situation in der Quantenmechanik, *Naturwissenschaften* **23**(48), 807 (1935).
- [27] M. Mirrahimi, Z. Leghtas, V. V. Albert, S. Touzard, R. J. Schoelkopf, L. Jiang, and M. H. Devoret. Dynamically protected cat-qubits: a new paradigm for universal quantum computation, *New J. Phys.* **16**, 045014 (2014).
- [28] F. Albarelli, M. G. Genoni, M. G. A. Paris, and A. Ferraro. Resource theory of quantum non-Gaussianity and Wigner negativity, *Phys. Rev. A* **98**, 052350 (2018).